Astron. Astrophys. 348, 978–989 (1999)

ASTRONOMY AND ASTROPHYSICS

The optical nebulae around the symbiotic Miras He 2–147, HM Sagittae and V1016 Cygni⋆

R.L.M. Corradi[1], **O.E. Ferrer**[2,3], **H.E. Schwarz**[4], **E. Brandi**[2,5], **and L. García**[2]

[1] Instituto de Astrofísica de Canarias, c. Via Lactea S/N, E-38200 La Laguna, Tenerife, Spain
[2] Facultad de Ciencias Astronómicas y Geofísicas, Universidad Nacional de La Plata, Paseo del Bosque, 1900 La Plata, Argentina
[3] Consejo Nacional de Investigaciones Científicas y Técnicas, Argentina
[4] Nordic Optical Telescope, Apartado 474, E-38700 Sta. Cruz de La Palma, Spain
[5] Comisión de Investigaciones Científicas de la Provincia de Buenos Aires, Argentina

Received 12 March 1999 / Accepted 28 June 1999

Abstract. We present narrowband images and [NII]λ658.3 nm spectra, obtained under sub–arcsec seeing conditions, of the extended nebulae around the symbiotic Miras He 2–147, HM Sge, and V1016 Cyg. The main results of this study are:

– The nebula around He 2–147 is a ring expanding with a velocity of $\sim$100 km s^{-1} which is inclined at $\sim 55^\circ$ to the line of sight. The kinematical age of the ring is between 220 and 340 yrs, depending on the adopted distance, and its size is of the order of 10000 a.u.
– The bulk of the [NII] core emission of HM Sge is produced in an extended circumbinary region which, along the North-South direction, has a size of 0.″4, much larger than the binary orbit.
– HM Sge possesses a curved, collimated string of knots extending out to a distance of about 9″, with a fainter counterpart on the other side of the central star. We discuss the possibility that it is the result of a fast collimated wind from the white dwarf and (precessing) accretion disc. If so, its age would be $\sim 500 \cdot D_{kpc}$ yrs, where D_{kpc} is the (poorly known) distance to HM Sge in kpc.
– The [NII] core emission of V1016 Cyg is resolved into two blobs separated by 59$\pm$5 km s^{-1} and by 0.″40$\pm$0.″06 (extrapolated to P.A.=$+80^\circ$), which are identified with the kinematical features found by Solf (1983) in 1982. We compute an upper limit to their proper motions in the last 15 yrs, and show that they are not ejecta from the 1965 outburst.
– V1016 Cyg is surrounded by a 20″ elongated nebula, whose major axis is at P.A.=$+45^\circ$. Along this direction, we find an extended kinematical feature with projected velocities of about $\pm$30 km s^{-1} which extends 3″ from the centre, ending on the SW side in a low–ionization knot.

These data provide unique information on the occurrence, geometry and dynamics of ancient mass loss events from these systems, which are likely to be related to unrecorded outbursts of their hot components. We set constraints on the recurrence time between outbursts and the accretion rates of the hot components, using the observed high incidence of nebulae among symbiotic Miras, the observed multiple nebulae, and the maximum observed age of the nebulae. We also discuss the implications of the observations of these nebulae for the theories of formation of aspherical planetary nebulae.

Key words: stars: binaries: symbiotic – stars: individual: He 2-147; HM Sge; V1016 Cyg – stars: mass-loss

1. Introduction

Our knowledge about the nebular environment of symbiotic stars has improved significantly in recent years. Basic information about the morphology of the innermost regions of these interacting binaries was obtained by means of radio observations (see the list of references in Corradi et al. 1999), ground–based long–slit spectroscopic imaging (Solf 1983, 1984), and HST imagery (Paresce & Hack 1994). In addition, ground–based CCD imaging using specific narrow–band filters allowed us to discover extended ionized nebulae with sizes typical of planetary nebulae (up to more than one parsec). An updated list of radio and optical images of nebulae around symbiotic stars, as well as a general discussion of their properties, is given in Corradi et al. (1999).

The study of these nebulae provides basic information about the geometry, dynamics, and history of the mass loss from symbiotic stars over the last few thousand years. The nebulae are the result of the combination of several processes: slow winds from the cool giants, fast winds and ejecta from the hot components during and between eruptions, photoionisation from the hot stars and/or shock excitation in colliding winds and high velocity outflows.

Send offprint requests to: R. Corradi (rcorradi@ll.iac.es)

⋆ Based on observations obtained at the 3.5m NTT telescope of the European Southern Observatory, and at the 2.6m NOT telescope operated on the island of La Palma by NOTSA, in the Spanish Observatorio del Roque de Los Muchachos of the Instituto de Astrofísica de Canarias.

Some spectacular ionized optical nebulae around symbiotic stars were studied in detail in the past, such as R Aqr (Solf & Ulrich 1985, Paresce & Hack 1994 and references therein), He 2–104 and BI Cru (Corradi & Schwarz 1993), which belong to the class of symbiotic stars containing a Mira variable and a hot white dwarf. These systems show one or two large bipolar nebulae which are thought to be composed of the Mira wind, ejected into a highly aspherical configuration because of the binary interactions and re–shaped by fast winds from the hot components during outbursts which occurred between several hundred and a few thousand years ago (cf. Corradi & Schwarz 1997). The study of these nebulae is not only important for understanding the phenomena which occur within a few astronomical units from symbiotic stars, but is also relevant for other astrophysical fields, such as planetary nebulae (PNe), novae and supernovae, in which the role of binary interactions in shaping the stellar outflows is thought to be important, but whose observational evidence is scarce, or lacking completely.

Some symbiotic Miras are known to have undergone an energetic, long lasting and slowly decaying outburst in their recorded photometric history. They are called symbiotic novae; a complete list is given by Munari (1997). We present here a morphological and kinematical study of the extended nebular environment of three of them: He 2-147, HM Sge and V1016 Cyg. The nebula around He 2–147 was discovered by Munari & Patat (1993). A preliminary report of the detection of optical ionized nebulae around HM Sge and V1016 Cyg with sizes up to fifty times larger than previously known was given in Corradi & Schwarz (1997) and Corradi et al. (1999).

2. Observations

An [NII] image and long–slit spectra of He 2–147 in the same spectral region were obtained with the 3.5m NTT at ESO La Silla, Chile, using the EMMI multimode instrument. With the TEK 2048^2 CCD ESO#36, the spatial scale of the instrument was $0\farcs27$ pix^{-1}. The central wavelength and full width at half maximum (FWHM) of the [NII] filter used for imaging were 658.8 nm and 3 nm. One spectrum of He 2–147 across the central source at P.A.=$+3^\circ$ was obtained in 1996 with EMMI in the long–slit high–resolution mode (Corradi et al. 1996), providing a reciprocal dispersion of 0.004 nm pix^{-1}, and a spectral resolving power $\lambda/\Delta\lambda$=55000 with the adopted slit width of $1\farcs0$. Another spectrum with a perpendicular slit (P.A.=-90°) was taken in 1999, and has a reciprocal dispersion of 0.007 nm pix^{-1} and a spectral resolving power of 35000. For this second spectrum, EMMI was used in standard echelle mode, so that the slit length was limited to $3\farcs$ Details about the observations are given in Table 1. Images and spectra were reduced in a standard way using IRAF and MIDAS.

HM Sge and V1016 Cyg were observed at the 2.6m Nordic Optical Telescope (NOT) at the ORM, La Palma. Images were taken using the BroCam2 direct camera in 1996 and the ALFOSC instrument in 1997, both using a Loral 2k x 2k CCD but with a scale of $0\farcs11$ and $0\farcs19$ per detector pixel, respectively. The central wavelength and FWHM of the filters used at the NOT are: [OII] (372.5/2.9 nm), [OIII] (501.2/3.0), [OI] (631.1/3.0), Hα continuum (650.7/2.8), and [NII] (658.9/0.9). In the following, we will therefore indicate with the symbols above the emission in the nebular lines [OII]$\lambda\lambda$372.7,372.9 nm, [OIII]λ500.7, [OI]λ630.0, [NII]λ658.3, and the continuum emission (Hα cont.) shortwards of [NII]λ654.8 nm. These latter images were used to subtract the continuum and the field stars in the [NII] frames. The objects identified as field stars were also removed from the other emission–line images using the task *imedit* in IRAF.

Long–slit, high–resolution spectra of HM Sge and V1016 Cyg were obtained at the NOT using the echelle spectrograph IACUB (Mac Keith et al. 1993). The detector was a Thompson THX31156 1024 CCD, giving a spatial scale of $0\farcs14$ pix^{-1}. To increase the signal–to–noise ratio, 2×2 binning was done along both the spatial and spectral directions. The projected slit width was $0\farcs65$, providing a spectral resolution of 30000, with a reciprocal dispersion of 0.009 nm per binned pixel. The slit of the spectrograph was positioned both on the central star, and offset to cover specific regions of the nebulae. Exposure times, slit position angles and offsets are given in Table 1.

Both the NTT and NOT spectra cover a narrow region (one echelle order) including the Hα and [NII]λ658.3 lines. Note that almost all the images and spectra presented in this paper were obtained under sub–arcsec seeing conditions (see Table 1).

Table 1. Log of the observations

Images

object	date	filter	exp. time (sec)	seeing
He 2–147	26.4.96	[NII]	180	$0\farcs9$
HM Sge	4.6.96	[NII]	90, 300, 900×2	$0\farcs6$
	4.6.96	Hα cont.	300	$0\farcs6$
	16.7.97	[OII]	120, 2400×2	$1\farcs0$
	16.7.97	[OIII]	60, 300	$0\farcs9$
	16.7.97	[OI].	60	$0\farcs8$
V1016 Cyg	4.6.96	[NII]	300×3, 1200×2	$0\farcs6$, $0\farcs8$
	4.6.96	Hα cont.	90	$0\farcs7$
	16.7.97	[OII]	120, 1200×2	$0\farcs9$
	16.7.97	[OIII]	240	$0\farcs9$
	16.7.97	[OI]	60	$0\farcs9$

Long–slit spectra

object	date	P.A.(°)	offset*	exp. time (sec)	seeing
He 2–147	26.4.96	+3	centred	1200	$0\farcs9$
	27.4.99	–90	centred	900	$1\farcs1$
HM Sge	19.7.97	–5	centred	300, 600×2	$0\farcs7$
	19.7.97	–120	$2\farcs6$N,$1\farcs5$W	1200×2	$0\farcs7$
	19.7.97	+4	$4\farcs0$N,$3\farcs6$W	1800×2	$0\farcs7$
V1016 Cyg	19.7.97	+45	centred	300, 1200×2	$0\farcs8$
	19.7.97	+45	$1\farcs8$S,$1\farcs8$E	2400	$0\farcs8$

* Slit offsets are given in arcseconds from the central star toward North (N), South (S), East (E), or West (W). Seeing values are FWHM and are measured directly from the images or spectra.

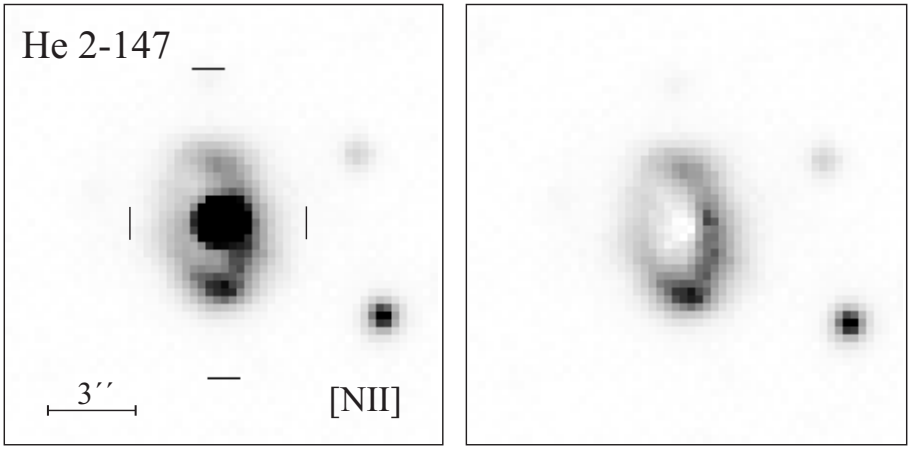

Fig. 1. The [NII] image of He 2-147, on a linear intensity scale, before and after subtraction of the central star emission. North is at the top, East to the left. The slit was positioned through the central star at P.A.=+3°; its location and width are indicated by lines on either side of the object.

3. He 2–147

Henize 2–147 is a symbiotic star containing a Mira with a pulsational period of about 375 days (Whitelock 1988). A complete list of works on this object is given in Munari & Patat (1993). According to Munari (1997), He 2–147 is a template case of a symbiotic nova whose PN–like spectrum (which is typical of the outburst phase of these systems) has "retreated" to the blue part of the spectrum leaving the red region dominated by strong TiO bands and continuum from the cool star (which is instead characteristic of the quiescent phase of symbiotic novae). No historical record of an outburst of He 2–147 exists.

3.1. Morphology and kinematics

In our [NII] image (Fig. 1), the nebula around He 2–147 has the shape of an elliptical ring, which is better appreciated after removing the emission from the central star (right box). The removal of the star was done by subtracting the average point spread function determined from field stars and normalised to the intensity of the central star. The ring is fainter on its eastern side than on the western one. In the image, the nebula is $4\farcs5\times2\farcs7$, measured at the peaks of the [NII] emission along its long and short axes.

The long-slit spectra of He 2–147 obtained at P.A.=$+3°$ (long axis of the ring) and P.A.=$-90°$ (short axis) are displayed in Fig. 2. The ring is probably due to emission from ionised gas and not reflected light from the core of the image, since its [NII]/Hα ratio is remarkably larger than in the core, a fact which is typical of many bipolar PNe (eg. Perinotto & Corradi 1998). The peak–to–peak size of the ring, as deduced from the spectra, is of $4\farcs4\times2\farcs0$, the latter value being quite uncertain since the emission from the edges of the ring in the spectrum at P.A.=$-90°$ is not well resolved from the continuum emission from the core. If we assume that the observed nebula is the projection on the sky of a circular ring (torus), from the average axial ratios measured in the image and spectra we derive an inclination (angle between the line of sight and the axis of the ring) around $55°$.

Heliocentric radial velocities corresponding to the different regions of the ring were measured by extracting the [NII] profile

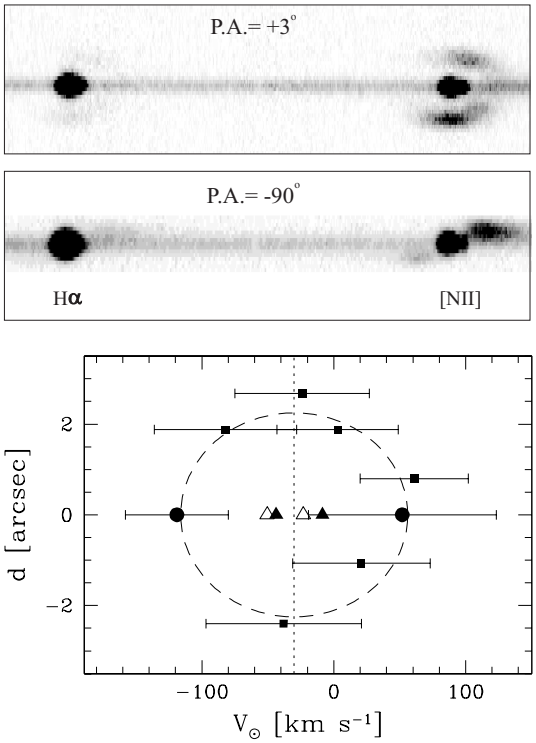

Fig. 2. Above, the long axis spectra of He 2–147 (on a linear scale). The spatial direction is the vertical one, while wavelengths increase along the horizontal direction. In the lowest box, the [NII] position–velocity plot for the ring (filled circles and squares) and the core (filled and empty triangles for [NII] and Hα, respectively). Heliocentric radial velocities are plotted as a function of the projected distance from the star along the vertical (long axis) direction (circles refer to the spectrum at P.A.=$-90°$, squares to that at P.A.=$+3°$). "Error-bars" indicate the FWHM of the [NII] emission. The vertical dotted line indicates the adopted systemic velocity, while the dashed ellipse is the velocity field expected for an inclined, expanding ring with parameters as adopted in the text.

at selected positions along the slits. In the long axis spectrum (P.A.=$+3°$), even though the $1\farcs0$ slit is narrower than the width of the nebula, the signal detected at all points is affected by non-negligible contamination from the whole ring, especially

from its western side. Extracting horizontal spatial profiles in the star–subtracted image shows in fact that the contribution to the spectrum of the emission from the western edge of the ring is substantial at all slit positions except for the one crossing the star (in this latter point, however, there is still some contamination). Note also that the effect is enhanced by the telescope tracking corrections. We then assume that the velocity field at P.A.=$+3^\circ$ represents that of the ring, except for the two points along its short axis, whose velocities are best taken from the spectrum at P.A.=-90°. The velocity separation of these latter points is 170 km s^{-1}.

We plot the observed radial velocities in the lower box of Fig. 2 as a function of the distances from the star projected onto the major axis of the ring. The observed velocity field is fully consistent with the hypothesis that the observed structure is the projection of a circular ring expanding with a space velocity of 105 km s^{-1} (we use the adopted inclination of 55° as computed from the apparent axial ratio). The kinematical fit is indicated by a dashed line in Fig. 2. Knowing the size and velocities, a kinematical age of 100$\cdot D_{kpc}$ yrs is obtained, where D_{kpc} is the distance to He 2–147 in kpc.

Note that the computed velocities in the ring should be given errors which are substantially larger than the real spectrograph resolution: this is because the signal from the nebula is faint, but also because the [NII] line profiles are strongly broadened, with FWHMs of up to 140 km s^{-1} (indicated by the "error-bars" in the position-velocity plot). At least partially, the high velocity dispersions measured at each position are due to mixing of the contribution of different kinematical regions of the shell, considering the poor spatial resolution in comparison with the very small size of the nebula. Nevertheless, substantial intrinsic broadening is also likely to exist.

We also extracted the Hα and [NII] line profiles of the unresolved core of the symbiotic system, by averaging the signal in the inner 1.″4. The [NII] core emission has a composite profile, that we fitted with a brighter component at $V_\odot$=-45 km s^{-1} and a fainter one at $V_\odot$=-10 km s^{-1}. Hα has a more symmetric profile, but the analysis also reveals the presence of a fainter, red-shifted bump, which is probably masked by the larger thermal broadening of the line as compared to [NII]. For Hα two components at $V_\odot$=-50 and $V_\odot$=-23 km s^{-1} (uncertain) were then measured. The core velocities are indicated by triangles in Fig. 2.

From the kinematical modelling above, we also derive an heliocentric systemic velocity for He 2–147 of $V_\odot$=-30 ± 8 km s^{-1} which coincides, within errors, with the mean velocity of the two components of the [NII] and Hα core emission. To our knowledge, this is the first measurement of the systemic velocity of He 2–147.

3.2. Discussion

Our image and spectra show that the nebula around He 2–147 is an annular structure whose axis is inclined $\sim$55° to the line of sight, and expanding at $\sim$100 km s^{-1}.

Among symbiotic Miras, R Aqr is also known to possess a large nebular ring expanding at 55 km s^{-1} (Solf & Ulrich 1985). Among PNe, there is a small number of objects which appear as thin, regular ellipses (e.g Schwarz et al. 1992). These objects received little attention in the past, until Bond et al. (1996) proved that the central stars of three of them are close binary systems, with orbital periods of a few days. Thus it appears that a common-envelope phase along the AGB can result in the ejection of matter strongly concentrated in an "equatorial" plane, as proposed by Soker (1997). Among novae, Slavin et al. (1995) pointed out that the slower novae often show equatorial ring morphologies (in addition to other structured components such as polar blobs), while faster novae are generally more spherical. Thus annular nebulae and various classes of binary systems such as post-common envelope binaries, slower classical novae, and also wide symbiotic stars seem to be linked. This last case would contradict the conjecture of Soker (1997) that ring nebulae are produced by close binaries which underwent a post–common envelope phase with stellar companions. From a theoretical point of view, it is expected that the plane of ejection is close to the orbital plane (e.g. Mastrodemos & Morris 1999). Therefore ring nebulae would provide a tool to determine basic parameters of binary systems, namely the inclination of the orbital plane and the position angle of the line of nodes. Alternatively, if all orbital parameters were known, they would constrain the mass loss geometry in binary stars (equatorial, meridional, or even inclined flows). More in general, a large fraction of PNe are characterised by having a brighter "equatorial" region and fainter "polar" extensions (e.g. Corradi & Schwarz 1995). These morphologies are supposed to originate in the interaction between a fast wind from the post–AGB central star and the slower and denser AGB remnant. If the slowly expanding envelope is characterised by densities which are moderately higher along some equatorial plane than in the polar directions, an elliptical nebula will then develop (Balick 1987). If the density contrast is larger, a bipolar nebula is instead created. In this view, ring nebulae can be considered as extreme cases, in which material in the polar directions and at intermediate latitudes (if any) is exceedingly tenuous, or has already vanished in the surrounding space. In the case of He 2–147, possible evidence of gas out of the equatorial plane might be suggested by the detection in our [NII] image of very faint nebular structures faraway from the ring of He 2–147, and/or by the substantial line broadening in the poorly resolved regions within the ring, which might measure the velocity of gas at intermediate latitudes. Deeper observations (and/or at higher spatial resolution) are needed to resolve this issue.

The expansion velocity of the ring of He 2–147 is notably high, one order of magnitude larger than the typical expansion velocity of the wind from an AGB star. If the ring is mainly composed of the Mira wind, then not only is it necessary that the binary interaction forces the Mira mass loss to be strongly concentrated in some "equatorial" plane, but an acceleration mechanism of the wind is also needed to accelerate the material to the high velocity observed. This might be provided by the interaction with a fast wind from the hot component.

The measurement of the systemic velocity of He 2–147 allows us to get an independent estimate of its distance from the Sun. He 2–147 is in fact located relatively close to the Galactic plane at a favourable longitude (l=328°) to obtain an estimate of its distance by assuming that it participates to the general circular rotation around the Galactic centre. Assuming a standard Galactic rotation curve (cf. Corradi & Schwarz 1995), the kinematical distance to the nebula is then computed to be 2.2 kpc, with a large uncertainty related to the simplistic assumptions in its derivation. Whitelock (1988) derived a larger distance of 3.4 kpc. The kinematical age of the nebula is then constrained to lie between 220 and 340 yrs, depending on whether the shorter or longer distance is adopted. Its size is between 0.05 and 0.07 pc. The nebula is therefore relatively young, possibly ejected in an outburst which occurred few centuries ago. So He 2–147 is a case the extended nebula provides information about, and the epoch of the occurrence of unrecorded nova–like eruptions.

He 2–147 is brighter on the west and south side, fainter in the east and north. It is tempting to assign these differences to extinction but this could only work for the W-E difference (red- and blue shifted respectively), with the outer face of the nebula having an absorbing layer. The N and S sides have basically zero radial velocities, and therefore the brightness differences in He 2–147 are probably caused by intrinsic density variations rather than by extinction.

As with the core of He 2–147, both the Hα and [NII] profiles were de-blended into two components, one bluer by 15–20 km s^{-1} than the adopted systemic velocity of the nebula, and the other redder by a similar but more uncertain amount. These velocities are typical of an undisturbed Mira wind, and might be produced in the portion of the wind from the cool giant which is ionized by the hot companion.

4. HM Sagittae

HM Sge is a symbiotic nova, which has been studied intensively in every accessible spectral band after the outburst of 1975 (Dokuchaeva 1976), in which the star brightened by about 6 magnitudes in the visual. Since then, its optical luminosity has only slightly decreased (Yudin et al. (1994). The circumstellar material around HM Sge was resolved by several authors at radio wavelengths (Richards et al. 1999 and references therein), and in the UV by HST imaging (Hack & Paresce 1993). Several kinematical features were also spatially resolved in the optical by Solf (1984), by means of ground–based, high resolution spectroscopy obtained at several position angles. From these data, Solf (1984) and Eyres et al. (1995) proposed the existence of a bipolar outflow from the system, expanding along the East–West direction and forming a small angle with the plane of the sky. More recent radio data allowed Richards et al. (1999) to refine this model, and to propose a wide biconical outflow arising from an inner, rotating torus/disc whose axis is projected EW and is inclined of 60° on the line of sight. The binary axis would be presently directed NS (Richards et al. 1999). Recent spectropolarimetric data, however, would rather indicate that the binary axis is presently at about P.A.=+120° (Schmid et al. 1999, in preparation).

Our star-subtracted [NII] and [OII] images of HM Sge are presented in Fig. 3, and the [NII] spectra in Fig. 4.

4.1. Morphology

The [NII] and [OII] images reveal the existence of a large nebula (30″ in [NII]) around HM Sge. Its morphology is very structured, and we distinguish three main components: the bright core, which is partially resolved in knots (left hand box in Fig. 3); a curved string of knots at intermediate brightness levels (right hand boxes); and a faint, more diffuse component (the faintest nebulosity in the central image) elongated roughly in the same direction as the intermediate nebula. The curved feature at intermediate brightness is observed both in [NII] and [OII] emission and is prominent in the North–West direction. On the other side of the central star, however, there are two knots (better seen in the [OII] light, and marked with arrows in the [NII] image) which are probably it's South–East counterpart.

In Fig. 3, we also present the 6 cm radio image of HM Sge (adapted from Eyres et al. 1995), which provides very valuable complementary information in the innermost regions which are not resolved in optical images. We do not show the HST UV image by Hack & Paresce (1993), since it offers very similar information to the 6 cm map. The most interesting features of the 6 cm map are the two bright ridges separated by 0.″16 which were interpreted to be the projection onto the sky of a circumstellar thick disc/torus (Eyres et al. 1995, Richards et al. 1999). Note that the open sides of this torus (i.e. the projection onto the sky of its symmetry axis) coincide with the direction of the curved collimated structure of our images. We will come back to this point in the following sections.

In our [OIII] and short [OI] images, no sign of the extended nebula is present, and the core is only marginally resolved. The object is clearly stellar in the Hα continuum image.

4.2. Kinematics: resolving the inner regions

The [NII] spectrum through the centre of HM Sge at P.A.=−5° is shown in the leftmost box of Fig. 4. Note that the 0.″65 wide slit was positioned nearly along the North–South direction, so that it includes all the 6 cm radio emission in Eyres et al. (1995). On the contrary, some of the elongated emission in the East–West direction detected at 18 cm is not included in our spectrum, such as the features labelled W and E by Eyres et al. (1995) and identified with the optical features at ±46 km s^{-1} in Solf (1984) (little contamination is expected because of seeing effects). Nevertheless, inspection of the radio maps shows that our spectrum at P.A.=−5° includes the region where the bulk of the nebular flux from HM Sge is produced.

These innermost regions are not resolved in our ground–based images. In the high-resolution spectra, however, the spatial location of *kinematically separated* regions can be obtained with an accuracy much better than the seeing value, as demonstrated by Solf (1983, 1984). In fact, at each wavelength (veloc-

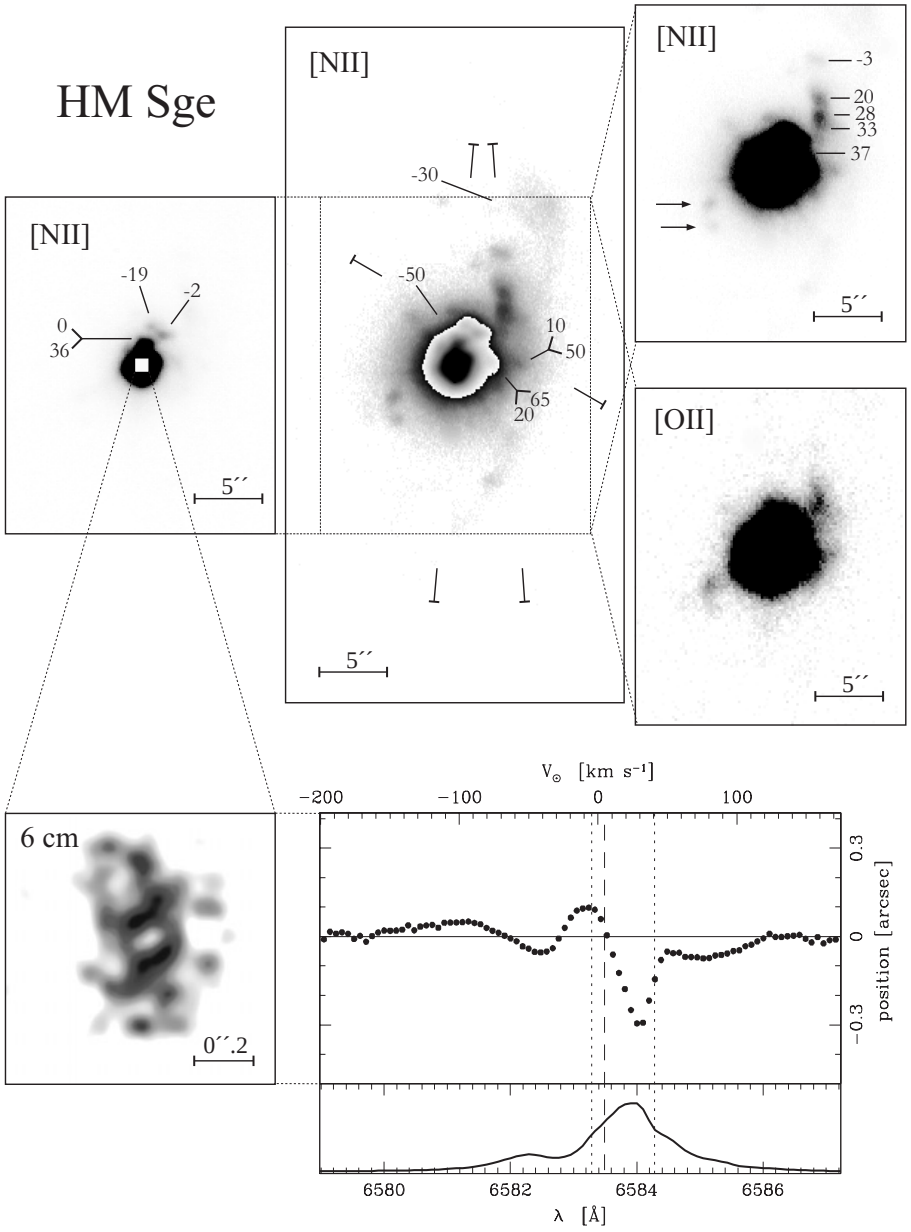

Fig. 3. At the centre, a logarithmic [NII] image of HM Sge, with two different intensity cuts for the inner and outer regions. North is at the top, East to the left. The locations of the slit used for spectroscopy are indicated by lines on either side of the object. Details of the inner regions are given in the left box, while the bended string of knots of intermediate brightness is highlighted in the [NII] and [OII] maps at the right (in a linear scale). In all images, the continuum and the field stars were removed. Radial velocities of individual features, corrected for the adopted systemic velocity, are shown as labels in the images. Below, the 6 cm radio map (Eyres et al. 1995). On the side, on the same spatial scale the [NII] core profile together with the deviations of the centre of the [NII] emission at each pixel-in-wavelength from the position of the continuum emission (see text).

ity) resolution element the centroid of the position of the [NII] emission can be determined with a typical accuracy of a fraction of a pixel. The procedure adopted was the following. We assume that the continuum emission is produced very close to the central stars. Its spatial position along the slit was accurately measured in the line–free regions of the spectrum on both sides of the [NII] line, and extrapolated by polynomial fitting to the wavelengths where the nebular [NII] emission dominates. This ensures removal of the geometric distortion of the 2–D spectra. The r.m.s. deviation from the fit was 0.″02. Then the spatial centroid of the [NII] emission at each wavelength pixel was measured by Gaussian fitting, which was found to be an adequate representation of the spatial profile at most wavelengths, and compared to the expected position of the continuum–emitting region.

Results are shown in the bottom–right box of Fig. 3, and compared to the radio maps. In the figure, we indicate with black circles the deviations of the centres of the [NII]–emitting zones from the extrapolated position of the continuum–emitting region, together with the [NII] line profile of the core of HM Sge obtained by integrating the emission over the innermost 1.″4. Significant spatial deviations are detected at several wavelengths. Features as close as 0.″05 from the centre can be resolved, and related to the multiple components which give rise to the complex profile of the integrated [NII] core emission. In particular, the peak of the profile and a large fraction of the [NII] flux come from a zone which has an extension of about 0.″4 and heliocentric radial velocities from about -5 to $+40$ km s^{-1} (profile between the dotted vertical lines in figure). There is a notable correspondence between this extended [NII] region and

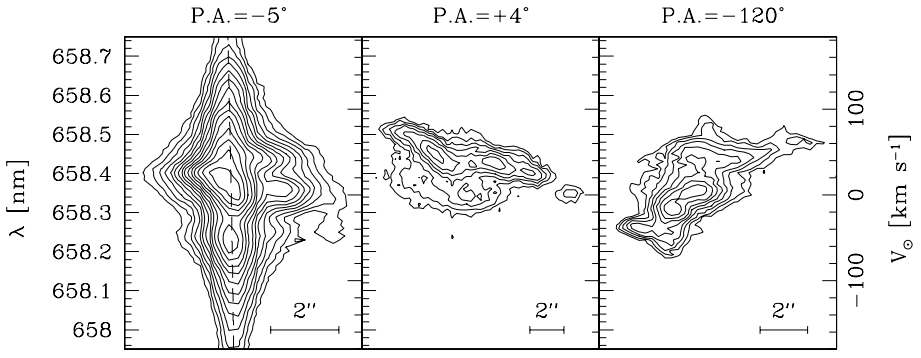

Fig. 4. Contour plot of the [NII] spectra of HM Sge. Successive levels increment of a factor $\sqrt{2}$. The spatial direction is the horizontal one (a scale bar of 2″ is provided in each spectrum), while wavelengths and velocities (both on a heliocentric reference frame) increase along the vertical direction. The dashed line in the leftmost plot indicates the extrapolated position of the continuum–emitting region (see text).

the radio maps, which enables us to relate morphological to kinematical features. We assume that the position of the continuum emission corresponds, within the errors, to the middle point between the inner ridges of the 6 cm map, where the central stars are supposed to be located, or equivalently to the UV peak, produced by the hot component. Then the resolved [NII] region would cover both the inner ridges and the southernmost knot seen in the 6 cm map. It is notable that the [NII] peak emission would then correspond to this knot; this might appear peculiar, but significant dust extinction could affect the [NII] emission from the innermost regions of the system. Note also that the resolved [NII] region, which extends preferentially to the South of the continuum emitting zone, nicely reproduces the NS asymmetry seen in the 18 cm radio map (but not in the 6 cm map, cf. Eyres et al. 1995). In the following, we adopt as the systemic velocity of HM Sge the wavelength at which the resolved [NII] region crosses the position of the extrapolated continuum emission. We obtain $V_{\odot}$=+5 km s^{-1}, and is indicated by a vertical dashed line in Fig. 3. Note that this value has to be considered as uncertain, because it might correspond to the velocity of circumstellar material which is seen in projection in the position of the central stars. Anyway, after removing the adopted systemic velocity, the radial velocities in the resolved [NII] region are consistent with the two components at $\pm$10 km s^{-1} found by Solf (1984): this velocity gradient from North to South might indicate rotation of the inner torus, as already pointed out by Solf (1984) and Eyres et al. (1995).

There are other components of the integrated [NII] profile at higher radial velocities whose centre is slightly offset from the continuum emitting region. One would be tempted to associate them with other features seen in the 6 cm radio map, but here we prefer to stick to the most basic and safest results.

4.3. Kinematics of the outer nebula

[NII] radial velocities at various positions within the extended nebula were measured by multi–Gaussian fitting in our three spectra. Radial velocities, corrected for the adopted systemic velocity of $+5$ km s^{-1}, are shown in Fig. 3 as labels attached to the corresponding morphological features. The velocity field of HM Sge is complex, reflecting the highly structured [NII] morphology. Components ranging from -50 km s^{-1} to $+65$ km s^{-1} with respect to the adopted systemic velocity are observed, but substantially different velocities (in some cases with sign reversal) can be found in the same region of the nebula, reflecting the presence of distinct morphological features projected onto the same position in the plane of the sky, or alternatively the existence of shocks which can result in very complex line profiles (e.g. Hartigan et al. 1987) which can be misidentified as different spatial velocity components.

A fairly regular velocity pattern can be traced only for the NW side of the curved collimated string of knots of intermediate brightness. There, radial velocities decrease systematically from a value of $+37$ km s^{-1} in the inner regions to -3 km s^{-1} in the outermost, detached knot. These data, together with the morphological information, suggest that the collimated structure is twisting in space, receding from the central stars in its inner regions, and then bending to the North and toward the plane of the sky (which is intersected at about the outermost knot) in its outer regions. This can result from episodic mass ejection characterised by a progressive variation of the direction of mass ejection within a cone of relative large aperture ($\geq 50°$) which intersects the plane of the sky and whose axis has a projected position angle around $-50°$. If we do the simple exercise of identifying the largest velocities observed ($+37$ km s^{-1}) with the maximum projected velocity expected for a cone of aperture $50°$ whose axis lies in the plane of the sky, we obtain deprojected expansion velocities of the order of 100 km s^{-1} or slightly less. Under the hypotheses above, the kinematical age of the outermost NW knot would be about $500 \cdot D_{kpc}$ yrs (the inner knots being of course younger). As with the features at $\pm$46 km s^{-1} found by Solf (1984) at a distance of about 0.″7 from the centre, and at a P.A.$\sim -60°$, they might be related to this collimated feature, since they have an orientation which is roughly the same and consistent radial velocities.

Finally, the faintest, outermost nebula has an orientation and morphology which are not very different from those of the string of knots of intermediate brightness, although it is much more diffuse (as expected for an older structure). We tentatively interpret it as the result of a previous mass loss episode from HM Sge with characteristics similar to the one producing the intermediate feature. Taking the size ratio between the two components as a measure of the age ratio, we obtain that the faintest nebulosity is $\sim$1.5 times older than the intermediate knotty structure.

4.4. Discussion

Based on the detailed physical structure deduced above for HM Sge, it is tempting to accept the interpretation of Eyres et al. (1995) and Richards et al. (1999) that the 6 cm radio features are the projection on the sky of a thick disc, and to conclude that the [NII] outflow occurs along its polar axis. In this hypothesis, the orientation of the polar axis of the system would be slightly different from that proposed by Eyres et al. (1995) and Richards et al. (1999). The large size of the disc ($160 \cdot D_{kpc}$ a.u., probably much larger than the binary separation) makes it difficult to assume that it precesses so as to cause the curving of the optical polar outflow. We would rather prefer an alternative scenario, adapted from the model by Morris (1987). Because of the binary interaction, the Mira wind distributes in a strongly flattened configuration along the orbital plane, forming an accretion disc around the hot component as well as an "excretion" disc around both stars (cf. also Mastrodemos & Morris 1999). The excretion disc would be identified with the bright emission at 6 cm. The collimated string of knots would be the result of a fast collimated wind from the hot component (white dwarf + accretion disc), interacting with the circumstellar material, its bending being provided by precession of the disc. This idea of a collimation mechanism very close to the white dwarf is in agreement with the HST images of R Aqr by Paresce & Hack (1994), in which it is shown that the collimation of the jet occurs within the innermost 15 a.u. from the central stars.

The scenario above, however, does not explain all observational data. First, it does not explain the distribution and kinematics of the knotty, irregular nebular [NII] emission in the inner regions (some features shows radial velocity components larger than in the curved string of knots). Secondly, recent measurements of Raman–scattering polarization (Schmid et al. 1999, in preparation) that the binary axis is at presently at about P.A.=$+120^\circ$. The hypothesis of a polar ionized outflow would require a position angle of the lines of nodes of the orbit of about 40°, and a large inclination ($\geq 60^\circ$). The spectropolarimetric data do not exclude this possibility, but would imply that the geometrical configuration stars–observer correspond to a large scattering angle ($\geq 150^\circ$), disfavouring measurements of a high polarization degree. An alternative to the scenario above is that the outer nebular material of HM Sge does not correspond to a 'polar' outflow, but is just the enhanced portion of an extended, irregular and knotty nebula.

The uncertainty in the distance to HM Sge, which ranges from 0.4 to 4 kpc according to different authors (cf. Richards et al. 1999), hinders the discussion of most of its physical properties. In any case, whatever distance is adopted, it is clear that the bulk of the [NII] emission from the core of HM Sge is produced in a region ($400 \cdot D_{kpc}$ a.u. along the N–S direction) which is much larger than the star separation which is commonly assumed. In the following, we adopt a distance of 2 kpc (Whitelock 1988) to obtain rough estimates of the size and kinematical ages of the outer structures. The total size of the faint, extended [NII] nebula of HM Sge would then be of 0.3 pc, i.e. typical of a planetary nebula. As for age, assuming the the collimated knots of intermediate brightness are indeed a precessing outflow directed not far from the plane of the sky, their kinematical age would be around 10^3 yrs. We also tentatively suggest that an additional, previous mass loss episode 1.5 times older has produced the outermost, faint nebular component. Thus the present observations may provide evidence for one or two ancient mass loss episodes from HM Sge, certainly not related to the outburst of 1975 but likely indicating the occurrence of previous ones.

The present data do not allow us to discuss in detail the dynamics of the innermost regions and to identify the different features with the ejecta of 1975, especially considering the high degree of complexity of the inner nebula. In this respect, the distance determination of 0.4 kpc by Solf (1984), the one by Eyres et al. (1995) of 3.2 kpc, and that by Richards et al. (1999) of 1 kpc, should be taken with extreme caution, since they are very model dependent and we have shown here that the geometry of the ejecta from HM Sge is complex.

5. V1016 Cygni

V1016 Cyg is another well–studied symbiotic Mira which suffered a nova–like outburst in 1965 (Fitzgerald et al. 1966). The circumstellar material around V1016 Cyg was resolved by radio and optical imagery (cf. Tables 2 and 3 in Corradi et al. 1999) and optical spectroscopy (Solf 1983, Bang et al. 1992).

5.1. Morphology

Our [NII] images (Fig. 5) reveal the existence of a $20''$ elongated nebula, whose major axis is oriented (both at small and large scales) at about P.A.=45°. At $2''.9$ from the centre and P.A.=224°, there is a knot (named A in the figure) which appears to be located inside a loop of emission departing from the elliptical core. Further out, a faint arc of emission, prominent on its eastern side, completes the apparent morphology of the low–ionization nebula. The [OII] image is very similar to the [NII] one, and it is not shown here. V1016 Cyg is spatially unresolved in our [OIII], [OI], and off-band (Hα continuum) frames.

The elliptical core and outer nebula align approximately with the $4''$ radio nebula detected at 6 cm by Kenny et al. (1993), as well as with the line connecting the innermost pair of knots, separated by $0''.1$, which in the 1.3 cm image of Taylor (1988) are resolved. On the contrary, the [OIII] image of Bang et al. (1992) shows no preferred axis of symmetry. Its large size, unusual for a high ionization species such as [OIII], together with the clear differences with respect to our [NII] and [OII] maps, suggest that the image (and spectra) by Bang et al. (1992) are partially contaminated by light from the central core scattered in a dusty, neutral circumstellar environment, or even scattered within the telescope/instrument or the terrestrial atmosphere (King 1971, Piccirillo 1973).

5.2. Kinematics

The [NII] spectra of V1016 Cyg at P.A.=$+45^\circ$ are presented in Fig. 6. As done for HM Sge, in the central spectrum we have ex-

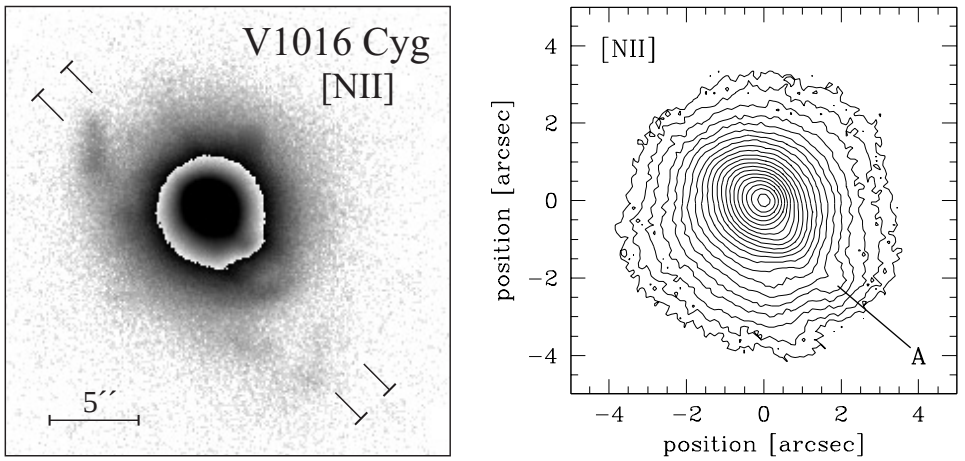

Fig. 5. The continuum-subtracted [NII] image of V1016 Cyg. North is at the top, East to the left. At the left, a logarithmic grey scale plot of the whole nebula, with two different intensity cuts for the inner and outer regions. At the right, a zoom of the inner 5″ from the centre in form of isointensity contours: successive levels increment of a factor $\sqrt{2}$.

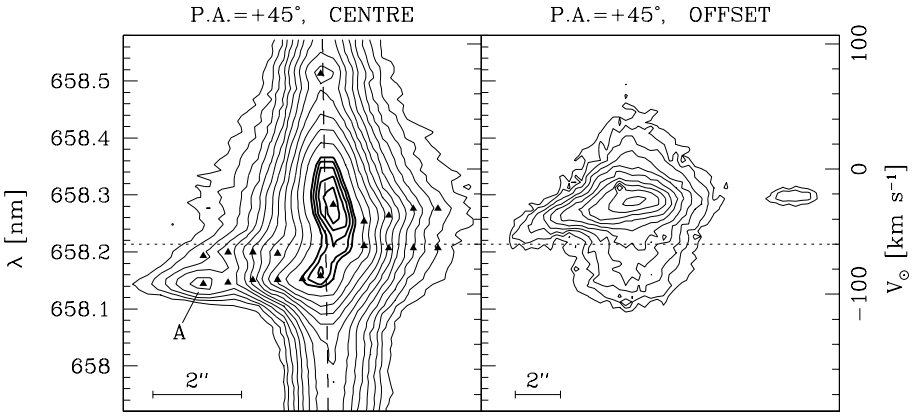

Fig. 6. The [NII] spectra of V1016 Cyg. Successive levels increment of a factor $\sqrt{2}$, except for the brightest region of the left box (thick contours) in which they are incremented of a factor 1.1 to show better the central components. The dashed line in the left plot shows the extrapolated position of the continuum–emitting region. Triangles indicate heliocentric velocities measured at selected positions along the slit, and the dotted horizontal line shows the adopted systemic velocity.

trapolated the position of the continuum to the [NII] wavelengths and compared it with the spatial location of kinematically resolved features. The [NII] peak emission in the central spectrum is resolved into two main components, separated in velocity by 59±5 km s^{-1} and spatially by 0.″33±0.″05. In the following, we adopt as the systemic velocity of V1016 Cyg the average between i) the middle value of the redshifts of these two inner components and ii) the centre of symmetry of the larger scale outflow indicated by triangles in Fig. 6 (and discussed below). We obtain $V_{\odot}$=−60±5 km s^{-1}.

The two inner components of our [NII] spectrum are identified with those found by Solf (1983) in spectra taken in 1982, 15 years before the present observations and 17 years after the outburst of 1965. From his data, obtained at several position angles, he inferred that the two kinematical "blobs" were in fact located along an axis at P.A.=+80°, and were separated by 0.″40 in space and by 51 km s^{-1} in velocity. Since we observed at a position angle different from 80°, the separation measured in our spectrum should be scaled by a factor $1/\cos(80^\circ - 45^\circ) = 1.22$ in order to remove the projection effects introduced by the 1–D slit and derive the actual separation. We obtain 0.″40±0.″06 for our 1997 data, which is the same separation as measured by Solf (1983). Thus there is no evidence that the blobs expanded since 1982: adopting an error of about 0.″05 for the measurements at each epoch, we estimate an upper limit of 0.″1 for the proper motions of the blobs in the last 15 yrs, i.e. a lower limit of 60 yrs for their kinematical age. This low expansion rate refutes the hypothesis of Solf (1983) that the blobs were ejected during the 1965 outburst, unless they slowed down dramatically in the last 15 years. Since their proper motions are basically undetermined and the distance to V1016 Cyg is poorly known (ranging from 0.6 to 6 kpc, cf. Bang et al. 1992), the age, inclination angle on the plane of the sky, and de-projected velocity of the blobs remain also undetermined. If the smallest distance is used (0.6 kpc), and we assume that the radial velocity difference reflects real motions of the blobs, then the upper limit on the proper motions in the last 15 yrs would constrain the inclination of the outflow to be within 20° of the line of sight.

In Fig. 6, we indicate with triangles radial velocities at various positions along the slit measured by multi-Gaussian fitting. On both sides of the central star, there are extended velocity features (indicated by the upper and lower horizontal series of triangles) departing from the inner blobs and extending out to about 3″ from the centre. These features are resolved into two velocity components. One is at zero radial velocity after removal of the systemic velocity, the other, symmetrical with respect to the centre, has a moderate radial velocity of a few 10s of km s^{-1}. On the SW side, this latter component connects the inner blob to knot A, showing a very slight increase in radial velocity from 25 to 30 km s^{-1}. On the other side of the central stars, there is a steep decrease of ∼15 km s^{-1} of the radial velocity just out of the position of the inner blob, but after that the extended velocity

feature gradually recovers the velocity of the inner blob. These features might indicate the presence of a two–sided, collimated outflow along the apparent major axis of the observed nebula. The spectrum also suggests that the inner blobs are directly related to the extended velocity pattern, but it remains unclear why the blobs are located at P.A.=$+80°$(Solf 1983), while the direction of the extended outflow and knot A is around P.A.=$+45°$. Also the zero velocity component is difficult to explain within this model.

The nature of the other morphological/kinematical components of V1016 Cyg is also unclear, due to the limited morphological and kinematical information. We note: *i)* in the spectrum through the central star, we detect a spatially unresolved component with a redshift of $+135$ km s^{-1} with respect to the systemic velocity (upper triangle at $V_{\odot}$=$+75$ km s^{-1}); *ii)* the innermost knots seen in the 1.3 cm image by Taylor (1988) are not detected in our spectrum; *iii)* the nature of the loop near the position of knot A and of the outer arc of emission is unclear, since we lack the kinematical information to reconstruct their spatiokinematical structure: the offset spectrum in Fig. 6 only allows us to say that the radial velocity of the NE extremity of the arc is $+40$ km s^{-1} with respect to the systemic velocity, while the central region of the spectrum suffers from contamination by light from the central source.

5.3. Discussion

Whatever the nature of the inner blobs, the present observations clearly define a main symmetry axis at P.A.=$+45°$ for the large scale outflow from V1016 Cyg. Limiting our discussion to axisymmetrical geometries, one possibility is that this axis is the projection of the polar axis of the system (presumably coinciding with the polar axis of the binary orbit), and so the inner velocity features ending in knot A indeed represent a collimated polar outflow. The line of nodes of the orbital plane would then be expected to be perpendicular to the polar axis at P.A.=$+135°$. Alternatively, the elongation of the inner nebula, as well as the outer [NII] loop and arcs may be the projection of a moderately inclined disc–like or ring–like distribution. This might in turn correspond to enhanced Mira mass loss in the equatorial (orbital) plane, as generally expected from theories (e.g. Mastrodemos & Morris 1999), resulting in a flattened circumstellar distribution seen at a moderate inclination. In this case, the line of nodes of the orbit would be at around P.A.=$+45°$, and knot A would be just a condensation, brightness enhancement or limb brightening effect in the orbital plane. The observed velocities, however, are not completely consistent with this hypothesis, since in the case of an expanding disc one would expect to have radial velocities which are decreasing with the distance from the centre, a fact which is not observed.

In the case of V1016 Cyg, the large uncertainties in the distance and in the projection effects prevent us to obtain reliable estimates of space velocities and kinematical ages of the various components of the nebula. Nevertheless, the upper limit on the proper motions of the innermost [NII] kinematical blobs in the last 15 years proves unambiguously that they are not direct ejecta from the outburst of 1965. As with the outer nebula, it has a projected size of $0.1{\cdot}D_{kpc}$ pc; adopting the moderate (a few tens of km s^{-1}) radial velocities measured in our spectra at all positions throughout the nebula as an order-of-magnitude estimate of the real expansion velocities, the kinematical age of the large nebula is estimated to be of the order of 10^3 yrs for a distance of $\sim$3 kpc (Whitelock 1988).

6. Constraints from the nebulae around symbiotic Miras

Including the three objects studied in the present article, information about the geometry, velocities, and timescales of large–scale outflows is now available for nearly all the extended nebulae known around symbiotic Miras (cf. Corradi et al. 1999). This wealth of data allows us to draw some general conclusions about the occurrence and properties of ancient mass loss events from these wide binaries, which in turn allow us to gain insight in the processes taking place in the innermost regions of these systems, as well as to discuss the implications for related astrophysical fields such as aspherical PNe.

6.1. Constraints on the time–scale for recurrent outbursts

In this section we will, somewhat speculatively, derive possible constraints on the recurrence times, accretion rates, and dynamical ages of these objects. To do that, we make the assumption that all the extended nebulae around symbiotic Miras are the result of (and thence the tracer) of outbursts of the hot component, be they the direct ejecta from the hot star, or the Mira wind swept up by fast, tenuous winds from the erupting white dwarfs. This is supported by the large expansion velocities of all nebulae, typically one order of magnitude larger than a Mira wind, so that fast winds are implicated.

Including all the information in the literature (cf. Corradi & Schwarz 1997), we report in Table 2 the kinematical ages of the extended nebulae known around symbiotic Miras. In most cases, the main limitation in computing the ages is the uncertainty in the distance. For HM Sge and V1016 Cyg, we have just adopted the distances by Whitelock (1988). In some cases (He 2–104 and R Aqr) there are two nebulae around the system, and we quote both. We also include in Table 2 the dates of the recent outbursts of HM Sge and V1016 Cyg, which according to our initial assumption will result in new extended ionised nebulae, which will become visible at some point in the future. For the objects with more than one nebula (He 2–104, R Aqr), or with nebulae and a recent outburst (HM Sge and V1016 Cyg), we derive from Table 2 recurrence times of nebula ejection of between 500 and 1000 yrs. These time scales can be related to those predicted by theory (cf. Sion 1997) for recurrent nova–like outbursts on the surface of the accreting hot companions. For high mass white dwarfs (>0.8 M$_{\odot}$), recurrence times of 500–1000 years are obtained with accretion rates around 10^{-8} M$_{\odot}$ yr^{-1}. For lower mass white dwarfs (~ 0.6 M$_{\odot}$), the typical post–AGB descendants of intermediate mass stars, these recurrence times are achieved with only slightly larger accretion rates, say a few 10^{-8} M$_{\odot}$ yr^{-1}. Considering a Mira mass

Table 2. Kinematical ages (rounded to the nearest hundred yrs) for ionized optical nebulae around symbiotic Miras (updated from Corradi & Schwarz 1997). Uncertain values are given as order-of-magnitude estimates and are indicated with a "$\sim$". D_{kpc} is a the adopted distance.

Object	Age (yr)	D_{kpc} (kpc)
BI Cru	2000	2.0
He 2–104	200	0.8
	900	
He 2–147	300	3.4
HM Sge	outburst in 1975	
	$\sim 10^3$	2.0
R Aqr	200	0.2
	700	
V1016 Cyg	outburst in 1965	
	$\sim 10^3$	3.3

loss rate of 10^{-5} $M_\odot$ yr^{-1} (cf. Mikolajewska 1997), the figures above would imply that less than 1% of the Mira mass loss is accreted in a typical system. The values above should be regarded as an upper limit to the accretion rate, since no systems are observed which possess multiple nebulae with an age difference (e.g. recurrence time) smaller than $\sim$500 years. For BI Cru, which exhibits a single, 2000 yr old nebula, and for other symbiotic Miras in which no nebulae are detected, the same reasoning as above would imply larger recurrence times, i.e. even smaller accretion rates.

From Table 2, we also see that the maximum observed kinematical age of a nebula around a symbiotic Mira is 2000 yrs. Considering that the detection rate for these extended nebulae is 40% (Corradi et al. 1999), one would be tempted to conclude that either the average life time of a symbiotic Mira is shorter than some 5000 yrs, or such systems *recurrently* produce an extended nebula more often than every 5000 yrs. The latter value would provide an upper limit to the recurrence times, i.e. a lower one to the accretion rates. Note, however, that observational selection effects may well favour the detection of active over quiescent systems, i.e. of objects in which one is likely to observe a nebula ejected in the relatively recent outburst; this makes the interpretation of the high detection rate of extended nebulae more difficult.

6.2. Connection with planetary nebulae: the effect of interactions in wide binaries

Symbiotic Miras give a nice practical demonstration of the nebulae resulting from the interaction of the different mass loss processes in wide binaries, a fact which has obvious implications for the theories about the shaping of PNe. Recent papers (e.g. Soker 1998, Garcia–Segura et al. 1999, Mastrodemos & Morris 1999) have in fact reopened the debate on whether highly asymmetrical mass loss on the AGB can be produced by single stars or that a binary system is needed. In particular, Garcia–Segura et al. (1999) argue that single stars with a sufficiently high mass (1.3 $M_\odot$) can achieve near–critical rotation rates during their late AGB phase, causing equatorially confined winds and hence bipolar planetary nebulae. Magnetic fields in the fast, post–AGB winds would also be important in shaping the nebulae. On the other hand, the hydrodynamical models by Mastrodemos & Morris (1999) show that a similar degree of anisotropy in the AGB wind can be achieved by gravitational interactions in detached binary systems with orbital periods as long as a few tens of years (thus partially matching the separations of symbiotic Miras, which are thought to be in the range 10–100 a.u., see e.g. Mikolajewska 1997).

Although they form quite a homogeneous class, the outflows observed in symbiotic Miras are very varied, although generally markedly axisymmetric. Including other objects from the literature, these outflows can take the form of bipolar nebulae (two lobes departing from an inner torus, He 2–104, BI Cru, and R Aqr), jets and collimated structures (R Aqr, HM Sge, and V1016 Cyg) and rings (He 2–147). The fact that among such binary systems nearly 40% of the nebulae is bipolar, and 100% is aspherical, while among the general population of PNe, only about 15% is bipolar (Corradi & Schwarz 1995), and some percentage is basically circularly symmetrical, indicates that binarity favours the formation of bipolar and aspherical nebulae. This strengthens the idea that any marked asymmetry in AGB and post–AGB mass loss is the natural outcome of binary interactions, confirming the conclusions of Soker (1997).

7. Summary

The present study has pointed out the existence of large–scale outflows from the symbiotic Miras He 2–147, HM Sge and V1016 Cyg. They have velocities of on the order of 100 km s^{-1} or less, sizes from few hundredths to few tenths of a parsec, and kinematical ages of hundreds of years. While mass ejection in He 2–147 seems mainly confined to a plane (the orbital one?), in HM Sge and V1016 Cyg we find evidence for the existence of elongated and collimated outflows.

Another notable result is that in both HM Sge and V1016 Cyg the [NII] core emission is produced in a volume much larger than that encompassed by the binary separation (around $400 \cdot D_{kpc}$ a.u. in both systems). Then this low–ionisation species is emitted from circumbinary material rather then from the ionised region between or close to the central stars, and is the best tracer of the large–scale outflows from these systems.

Acknowledgements. We thank Drs. Luca Pasquini and Giuseppe Cutispoto for donating the observing time at the NTT in 1999, Dr. Stewart Eyres for providing us with the radio images of HM Sge, and Drs. Hans Martin Schmid and Anita Richards for useful discussions on the intriguing geometry of the various outflows of HM Sge. One of us, RLMC, thanks the Observatory of La Plata for the hospitality during October of 1998, when most of this work was done. We also thank the referee for many useful comments, and for stimulating us to obtain new critical observations to test our proposed interpretation. The work of RLMC has been supported by a grant of the Spanish DGES PB97–1435–C02–01.

References

Balick B., 1987, AJ 94, 671

Bang M.K., Bode M.F., Ivison R.J., Meaburn J., 1992, MNRAS 256, 59

Bond H.E., Ciardullo R., Webbink R., 1996, Amer. Astron. Soc. Meet. 189, 9704

Corradi R.L.M., Schwarz H.E., 1993, A&A 268, 714

Corradi R.L.M., Schwarz H.E., 1995, A&A 293, 871

Corradi R.L.M., Mampaso. A., Perinotto M., 1996, ESO Messenger, ESO Messenger No.85, p. 37

Corradi R.L.M., Schwarz H.E., 1997, In: Mikolajewska J. (ed.) Physical processes in Symbiotic binaries and related systems. Copernicus Foundation for Polish Astronomy, Warsaw, p. 147

Corradi R.L.M., Brandi E., Ferrer O., Schwarz H.E., 1999, A&A 343, 841

Dokuchaeva O.D., 1976, Inf. Bull. Variable Stars, No. 1189

Eyres S.P.S., Kenny H.T., Cohen R.J., et al., 1995, MNRAS 274, 317

Fitzgerald M.P., Houk N., McCluskey S.W., Hoffleit D., 1966, ApJ 144, 1135

García-Segura G., Langer N., Rózyczka M., Franco J., 1999, ApJ, in press

Hack W.J., Paresce F., 1993, PASP 105, 1273

Hartigan P., Raymond J., Hartmann L., 1987, ApJ 316, 323

Kenny H.T., Taylor A.R., Davis R.J., et al., 1993, In: Davis R.J., Booth R.S. (eds.) Sub–arcsecond radio astronomy. Cambridge Univ. Press, Cambridge, p. 18

King I.R., 1971, PASP 83, 199

McKeith C.D., García López R.J., Rebolo R., et al., 1993, A&A 273, 331

Mastrodemos N., Morris M., 1999, ApJ, in press

Mikolajewska J., 1997, In: Mikolajewska J. (ed.) Physical processes in Symbiotic binaries and related systems.Copernicus Foundation for Polish Astronomy, Warsaw, p. 3

Morris M., 1987, PASP 99, 1115

Munari U., 1997, In: Mikolajewska J. (ed.) Physical processes in Symbiotic binaries and related systems.Copernicus Foundation for Polish Astronomy, Warsaw, p. 37

Munari U., Patat F., 1993, A&A 277, 195

Paresce F., Hack W.J., 1994, A&A 287, 154

Perinotto M., Corradi R.L.M., 1998, A&A 332, 721

Piccirillo J., 1973, PASP 85, 278

Richards A.M.S., Bode M.F., Eyres S.P.S., et al., 1999, MNRAS, in press

Schwarz H.E., Corradi R.L.M., Melnick J., 1992, A&AS 96, 23

Sion E.M., 1997, In: Mikolajewska J. (ed.) Physical processes in Symbiotic binaries and related systems. Copernicus Foundation for Polish Astronomy, Warsaw, p. 49

Slavin A.J., O'Brien T.J., Dunlop J.S., 1995, MNRAS 276, 353

Soker N., 1997, ApJS 112, 487

Soker N., 1998, ApJ 496, 833

Solf J., 1983, ApJ 266, L113

Solf J., 1984, A&A 139, 296

Solf J., Ulrich H., 1985, A&A 148, 274

Taylor A.R., 1988, In: Mikolajewska J., Friedjung Kenyon S.J., Viotti R. (eds.) The Symbiotic Phenomenon. Kluwer Academic Publisher, Dordrecht, p. 77

Whitelock P.A., 1988, In: Mikolajewska J., Friedjung Kenyon S.J., Viotti R. (eds.) The Symbiotic Phenomenon. Kluwer Academic Publisher, Dordrecht, p. 47

Yudin B., Munari U., Taranova G., Dalmeri I., 1994, A&AS 105, 169